High-resolution Mapping of North America's Mid-Mantle Reflectivity provides Evidence for Dehydration Melting

Steve A. B. Carr¹, Tolulope Olugboji^{1,2,3}, Jeffrey Park⁴, Shun-ichiro Karato⁴

3 4 5

6

1

2

- URSeismology Lab, Department of Earth and Environmental Sciences, University of Rochester, NY.
- ² Department of Electrical and Computer Engineering, University of Rochester, NY
- 7 Georgen Institute of Data Sciences, University of Rochester, NY
- 8 4 Department of Earth and Planetary Sciences, Yale University

9

10

11

12

13

14

15

16

17

18

19

20

21

22

23

24

Abstract

We investigate seismic discontinuities across the middle of Earth's mantle beneath a large seismic array that spans the North American continent. We provide robust constraints on the depth distribution, sharpness, and spatial variation of seismic discontinuities by processing high-resolution Ps-converted seismic waves (~0.5 Hz) through a novel denoising filter called CRISP-RF (*Clean Receiver function Imaging with Sparse Radon Filters*). In the upper mantle, above the mantle transition zone (MTZ), we observe a sharp velocity decrease at depths that vary from ~290 km to ~390 km. In the lower mantle, below the MTZ, we observe another sharp velocity decrease at depths that vary from ~800 km to 1,200 km. The lower-mantle discontinuities cluster at a depth of ~885 km, while deeper converters (> 1,000 km) are less likely. The spatial distribution of these seismic features appears stochastic, but we detect collocated upper-mantle and lower-mantle discontinuities only at 8% of observed locations. We interpret our results with a dehydration melting model, in which MTZ water is transported into either the upper or the lower mantle, but rarely simultaneously, during Earth's long history of subduction and mantle upwelling.

25

Plain Language Summary

We investigate the structure of Earth's mantle beneath North America using seismic waves generated from earthquakes. We reveal previously undetected features in Earth's mantle using a new technique called Clean Receiver function Imaging with Sparse Radon Filters (CRISP-RF). We observe scattering from anomalous mantle rocks, above and below the mantle transition zone (MTZ), where seismic wave speeds decrease sharply with depth. Above the MTZ, earthquake waves scatter at multiple depths between 290 and 390 kilometers, at seismic features that are not laterally contiguous over large distances. Below the MTZ, scattering occurs at depths of 800 to 1,200 kilometers with a concentration at ~885 kilometers. A vertical cross-section shows that only rarely (8%) does Ps scattering at the same geographical location occur both above and below the MTZ. Our findings support a model where water, transported deep into the Earth by tectonic processes, causes localized melting when it leaves the MTZ, either upward or downward. Our work provides new insights into the role of water in shaping Earth's deep interior.

1. Introduction

49

50

51

52

53

54

55

56

57

58

59

60

61

62

63

64

65

66

67

68

69

In a planet that dissipates heat through whole-mantle convection, discontinuities at depths with no mineral phase transition should be rare. Yet, growing seismological evidence suggests the presence of wide-spread reflectors above and below the mantle transition zone (MTZ: 410-660 km depth) with implications for chemical heterogeneity, water and volatile cycling, and mantle dynamics (Ballmer et al., 2015; Karato et al., 2020; Waszek et al., 2018). While the bounding MTZ discontinuities are understood to be caused by solid-state mineral phase transitions (Helffrich and Wood, 2001; Stixrude and Lithgow-Bertelloni, 2012; Tian et al., 2020), the details and causes of other discontinuities are still vigorously debated (Boschi and Becker, 2011; Deuss et al., 2013; Fei et al., 2023; Frazer and Park, 2024; Rudolph et al., 2015). In particular, the mid-mantle discontinuities detected between ~700-1,300 km have baffled a unified explanation (Frazer and Park, 2021; Hedlin et al., 1997; Schmandt et al., 2014; Waszek et al., 2018; Zhang et al., 2023). Multiple explanatory models have been proposed, including: dehydration melting (Bercovici and Karato, 2003; Frazer and Park, 2021; Schmandt et al., 2014), scattering from the underside of subducting slabs or the top of deflected mantle plumes (Kaneshima, 2019, 2018; Waszek et al., 2018; Yang and He, 2015), and the incorporation of hydrous basalts into the mantle (Bentham and Rost, 2014; Frazer and Park, 2024; Kaneshima, 2016). Innovative seismic techniques have furnished constraints on mid-mantle discontinuities, improving the detection thresholds, spatial coverage, and depth resolution, which is crucial for differentiating between interpretations. The earliest detections utilized converted body-waves

(Niu and Kawakatsu, 1997; Shen et al., 2003) and reverberations from Earth's surface to the core (Courtier and Revenaugh, 2008; Revenaugh and Sipkin, 1994). Subsequent regional and global studies have since expanded on these early findings, using receiver functions (Frazer and Park, 2021; Jenkins et al., 2017; Schmandt et al., 2014), and SS precursors (Kaneshima, 2023, 2019, 2016; Niu, 2014; Waszek et al., 2018; Zhang et al., 2023). The SS precursor method is used widely because it allows imaging in regions with poor station coverage. In fact, the scattering locations of SS precursors are heavily skewed towards oceanic regions near hotspots and subduction zones where station coverage is sparse (Bentham and Rost, 2014; Kaneshima, 2019, 2018; Waszek et al., 2018). In contrast, detections of mid-mantle discontinuities are rare across continents and are not limited to locations associated with mantle plumes or subduction (Frazer and Park, 2021; Jenkins et al., 2017; Niu, 2014). In this work, we test different explanatory models for mid-mantle seismic interfaces by providing robust constraints using a new high-resolution technique on large datasets from recent broadband seismic deployments. A key advance is that we improve the lateral coverage, depth resolution, and detection threshold on the depth, sharpness, and polarity of the velocity change. We do this by leveraging the dense station coverage across North America, and by applying a high-frequency body-wave technique. Some recent work have provided interesting results in the western US (Frazer and Park, 2021; Schmandt et al., 2014), however, a comprehensive study of the entire North American continent has not yet been conducted. Here we investigate mantle discontinuity structure across the transition zone using a new receiver function technique called CRISP-RF (Clean Receiver function Imaging using Sparse Radon Filters). This is a high-resolution approach that improves the detection threshold of

70

71

72

73

74

75

76

77

78

79

80

81

82

83

84

85

86

87

88

89

90

weak mantle reflectors buried in interfering signals from top-side transition zone reflections (Jenkins et al., 2017; Olugboji et al., 2023). We provide improved constraints on the presence, lateral distribution and polarity (velocity drop or increase) of the mantle reflectors across the entire North American continent. We then evaluate the competing models, e.g. hydrous melting or compositional layering, for their consistency with our new results.

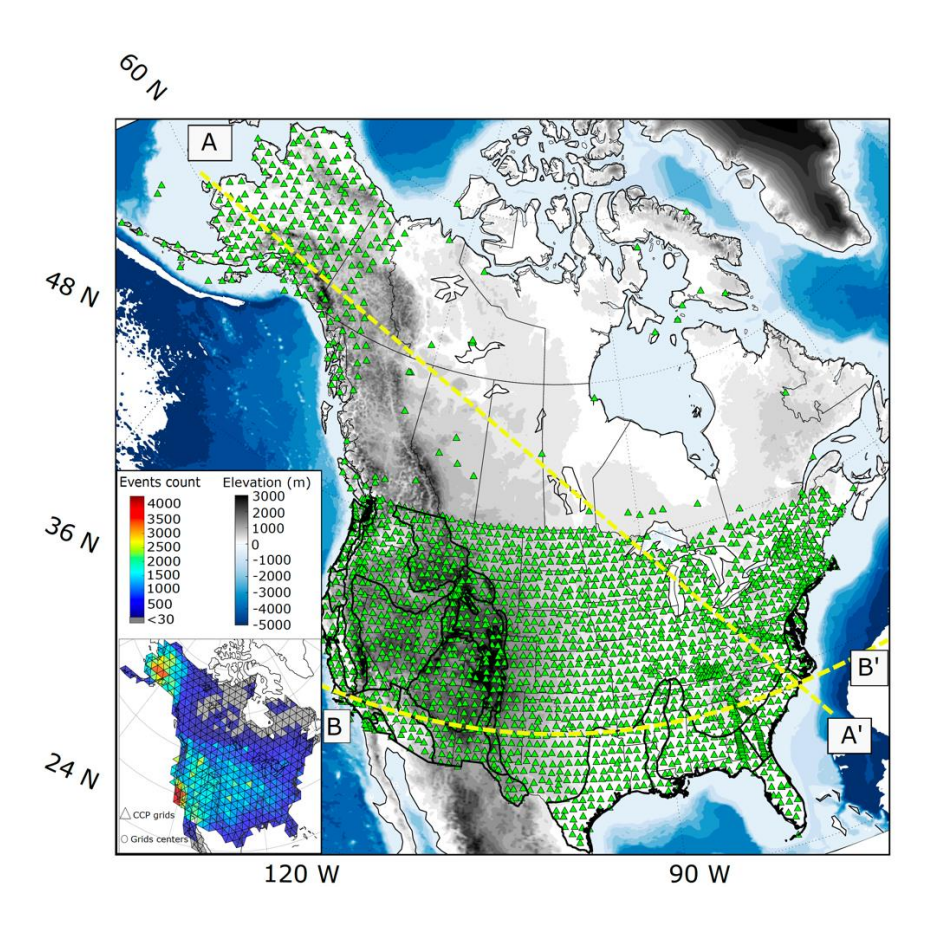


Figure 1. Station distribution and data coverage across North America. The seismic stations (green triangles) are overlaid on the background topography with two representative transects AA' and BB' used in describing the results (see Figure 3). The data coverage in the inset is organized into an equal-area triangular tessellation. The colors represent a count of all earthquakes passing through the same triangular patch with the same pierce point at 660 km.

Pg

2. Data and Method

2.1. Waveform-Data and Common Conversion Point Stacking

We analyze three-component waveforms of earthquakes (Mb > 5.5) recorded on broadband stations across North America. These stations are part of the US Transportable Array network as well as other major seismic networks deployed in the US, Canada, and Alaska (Figure 1). We start with an initial dataset of ~700,000 earthquakes and select ~103,000 of the highest quality waveforms for receiver function analysis. The seismograms are rotated from the geographic coordinate into the radial coordinates and filtered using a frequency cut-off of 0.5 Hz (Rondenay, 2009). We ensure uniform spatial coverage by employing a common conversion point (CCP) stacking scheme based on a triangular tessellation of the study area (Figure 1b and Figure S1). The earthquakes that pass through the same triangular patch (~1-degree equal sides) are stacked together. The pierce-points of the rays are calculated for depths of 350 km and 660 km, using a raytracing algorithm through the PREM model.

Receiver functions (RF) in each triangular cell are calculated using an extended-time multitaper cross-correlation technique (Helffrich, 2006). The time-domain coherence of the receiver functions are improved by stacking using the frequency-dependent coherence estimates (Park and Levin, 2016, 2000). The stacking is done using equally spaced 3-degree epicentral bins for earthquakes located between 30 and 90 degrees. We are interested in discontinuities not predicted by 1-D reference earth models such as PREM or ak135 (Dziewonski and Anderson, 1981; Kennett et al., 1995). We focus on identifying direct mantle conversions between 280 km and 1300 km (Ps delay time between 28 s to 130 s). When interpreting Ps-RFs at these depths, interference is possible from reverberations generated within the crust or from the top of the transition zone (e.g., Pp410p and Pp660p) (Jenkins et al., 2017; Olugboji et al., 2023). These larger-amplitude reverberations often mask signals from weaker conversions in the mantle and make their detection challenging (Figures 2a, c, and S2).

134

135

136

137

138

139

140

141

142

143

144

145

146

147

148

149

128

129

130

131

132

133

2.2. CRISP-RF Processing: Radon Filters and Migration

We improve the detection of low-amplitude mantle conversions by rejecting reverberations of comparable amplitude with the method of Clean Receiver function Imaging using Sparse Radon Filters (CRISP-RF) (Carr and Olugboji, 2024; Olugboji et al., 2023; Zhang and Olugboji, 2024). CRISP-RF is an imaging approach based on wavefield separation through selective backpropagation. Separability in the backward propagated Radon model is possible because of the unique travel-time curvature (second derivative of travel-time as a function of slowness) for converted and reverberated waves. This traveltime curvature is positive for a beam of upwardly traveling converted waves and negative for reverberated waves reflecting at a sharp interface that appears to be generated from a virtual source at the free surface (see Figure S2). The Radon model selects and isolates upward-propagating converted Ps waves arriving with positive travel-time curvature. A final forward-projection, using the inverse Radon transform, recovers a receiver-function dataset that is largely free of interfering multiples and is significantly denoised (See examples in Figures S3 and S4). Full details of the CRISP-RF methodology can be found in (Olugboji et al., 2023). A final post-processing step aligns the filtered receiver functions using an appropriate velocity model (PREM) for migration. Above the transition zone, we migrate to 410 km, and below the transition zone we chose a migration depth of 520 km. This migration process introduces an uncertainty of ~10-20 km in the interface depths, depending on the reference model used (see Figure S3).

3. Results: Discontinuities across the MTZ

We observe marked improvements in the receiver function stacks after filtering using CRISP-RF. Incoherent arrivals that are not related to direct conversions are effectively discarded. The detection of the MTZ discontinuities is pronouncedly improved. Secondary arrivals with negative amplitudes are more easily observed above and below the transition zone. Prior to the denoising steps, these signals are buried within incoherent noise and shallow-layer reverberations that transmit through a heterogeneous crust reflecting off the Moho or transmitting through the upper mantle before reflecting off the top of the mantle transition zone (compare Figures 2 a, c to Figures 2 b, d. See also Figure S6 b and c). By contrast, the filtered and migrated receiver functions are free of these complex scattered phases. A comparison of filtered and unfiltered Ps-RFs shows that the MTZ discontinuities are now clearly observed (positive amplitudes in Figure 2b and 2d).

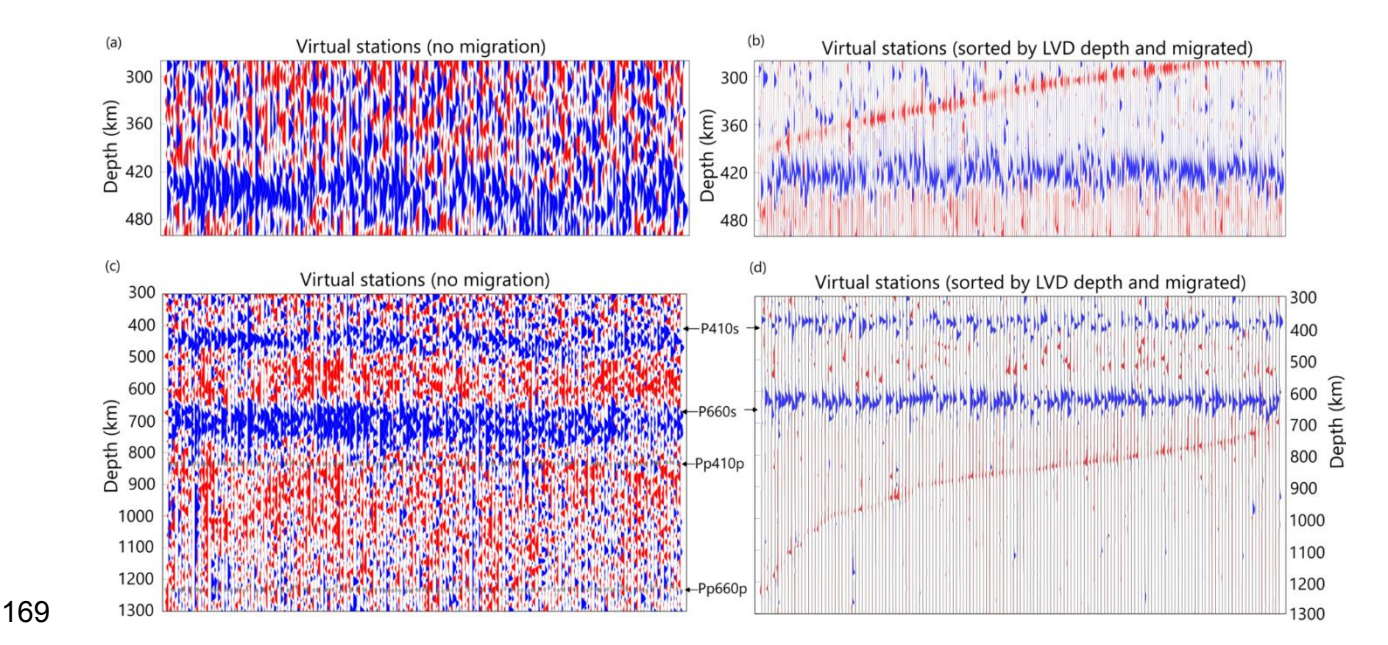


Figure 2. Improved detection of mantle discontinuities with CRISP-RF. (Left) Noisy Ps-RFs without CRISP-RF processing and no migration applied. Each trace is a stack using waveforms common to a single cell in the triangular tessellation of Figure 1 inset. (Right) Denoised Ps-RFs after CRISP-RF processing with migration and sorting. Panel (b) is migrated to 410 km and (d) is migrated to 520 km, all based on the PREM velocity model. Results are shown for discontinuities above the transition zone (a and b) and below the transition zone (c and d). See Figure S3 for details.

An ordered profile of the filtered Ps-RF traces reveals a new discontinuity above the transition zone. These are marked by negative amplitudes generated from a sharp velocity decrease located at a depth that varies from ~290 km to ~390 km (Fig. 2b). These arrivals are not a side-lobe precursor of the P410s arrival because we do not observe a symmetric side-lobe below the `410', only a negative pulse above it. The time-separation of this negative Ps pulse relative to the positive Ps pulse from the 410-km discontinuity varies geographically across North America, a behavior inconsistent with a signal-processing artifact. We also observe a similar discontinuity below the 660-km interface of the MTZ which is weaker than the upper mantle discontinuity (Figure 2d). Each of these arrivals has been carefully and manually inspected to ensure that they are direct arrivals (not spurious reverberations). We further investigate the spatial patterns of these discontinuities using two major transects (Figure 3).

The goal is to identify regional patterns in the depths of the observed low-velocity discontinuities (LVDs).

3.1 Low-Velocity Discontinuity Above the MTZ

The strongest signals in our filtered Ps-RFs, apart from the bounding MTZ discontinuities, are from the low-velocity discontinuity above the '410'. When sorted, this discontinuity can be detected in a range from 5 km to 120 km above the MTZ, with a near-continuous distribution of depths (Figure 2b). Geographically, however, the depth of this scattering horizon varies somewhat randomly along transects A-A' and B-B'. The depth distribution of the supra-MTZ velocity inversion shows no systematic variation with distance (Figure 3 c and 3d). In parts of Alaska and Canada, we observe fewer interface detections compared to the Northeastern US. The spatial variations in depths and detection frequency suggest complex underlying processes. Our results, compared to other regional and global compilations (Hier-Majumder and Tauzin, 2017; Tauzin et al., 2010; Tauzin and van Der Hilst, 2013), cover a more extensive footprint across North America.

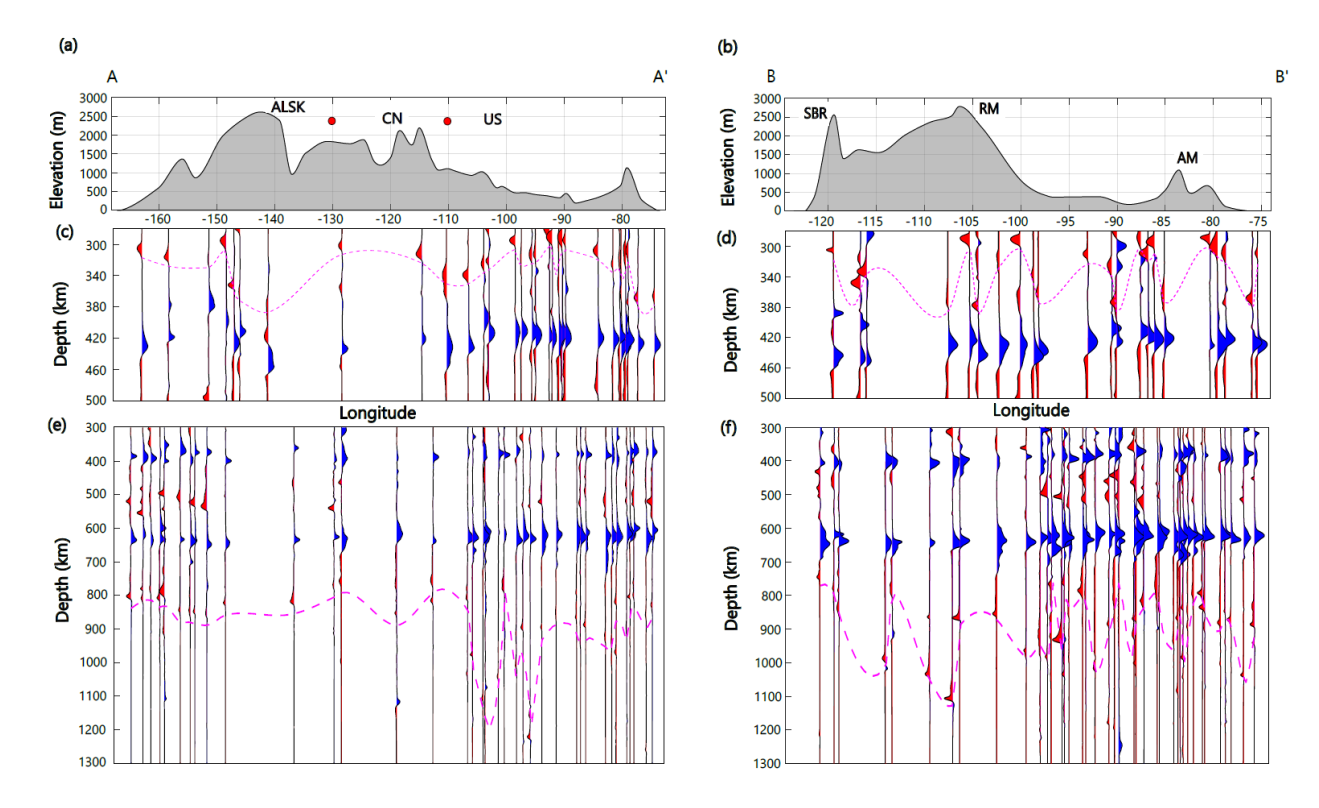


Figure 3. Filtered and migrated Ps-RFs stacks organized along two transects spanning North America. (a and b) Topography along transects AA' and BB'. Transect A-A' is oriented north-west to south-east starting from Alaska (ALSK), traversing Canada (CN) and terminating in south-eastern US. Transect B-B' is oriented east-west starting in California crossing the Southern Basin and Range (SBR), Rocky Mountains (RM), and ending at the southern tip of the Appalachian Mountains (AM). (c and d) The negative (red) amplitudes indicate a low-velocity discontinuity above the transition zone. (e and f) Smaller negative amplitudes below the transition zone indicate a much weaker velocity drop in the mid-mantle.

3.2. Low-Velocity Discontinuity Below the MTZ

Below the MTZ, we observe another low-velocity discontinuity (Figure 2d). Along transect A-A', we observe this discontinuity at a relatively consistent depth (Figure 3e). Underneath Alaska, it is located ~200 km below the transition zone, at a depth of ~800 km. As we move southward, along A-A', towards the eastern US, the pattern becomes more complex. Underneath the Canadian region, the discontinuity becomes sparse, slightly shallower, and more gradational. These results may be influenced by limitations in data coverage relative to the contiguous US and Alaska (see Figure 1 inset and S1). Along transects B-B', moving from west to east, we note a rapid deepening of the

discontinuity from ~800 km to 1,100 km at its deepest point below the highest peaks of the Rocky Mountains at the surface. At this location, and further east, we observe a shallower discontinuity at a depth~ 900 km. Further east approaching the southern tip of the Appalachian Mountains, the interface becomes more heterogeneous showing up as multiple negative Ps-RF arrivals that span a depth range of ~300 km (Figure 3f). This lack of coherence in the depth is in sharp contrast to the results underneath Alaska and in the southern US, east of the Rocky Mountain orogen.

3.3. Spatial Distribution of the LVDs

We investigated the spatial and depth coherence of the newly detected low-velocity discontinuities across North America. Our study region was divided into 809 triangular cells (Figure 1 inset) and after rigorous and selective data and CRISP-RF processing, only 455 cells (~56% by surface area) produced stable and interpretable results (Figure S5). Amongst these, 228 cells yielded a clear LVD detection, excluding ambiguous detections (Figures 4a and 4b). While this is only 28% of our study area, it

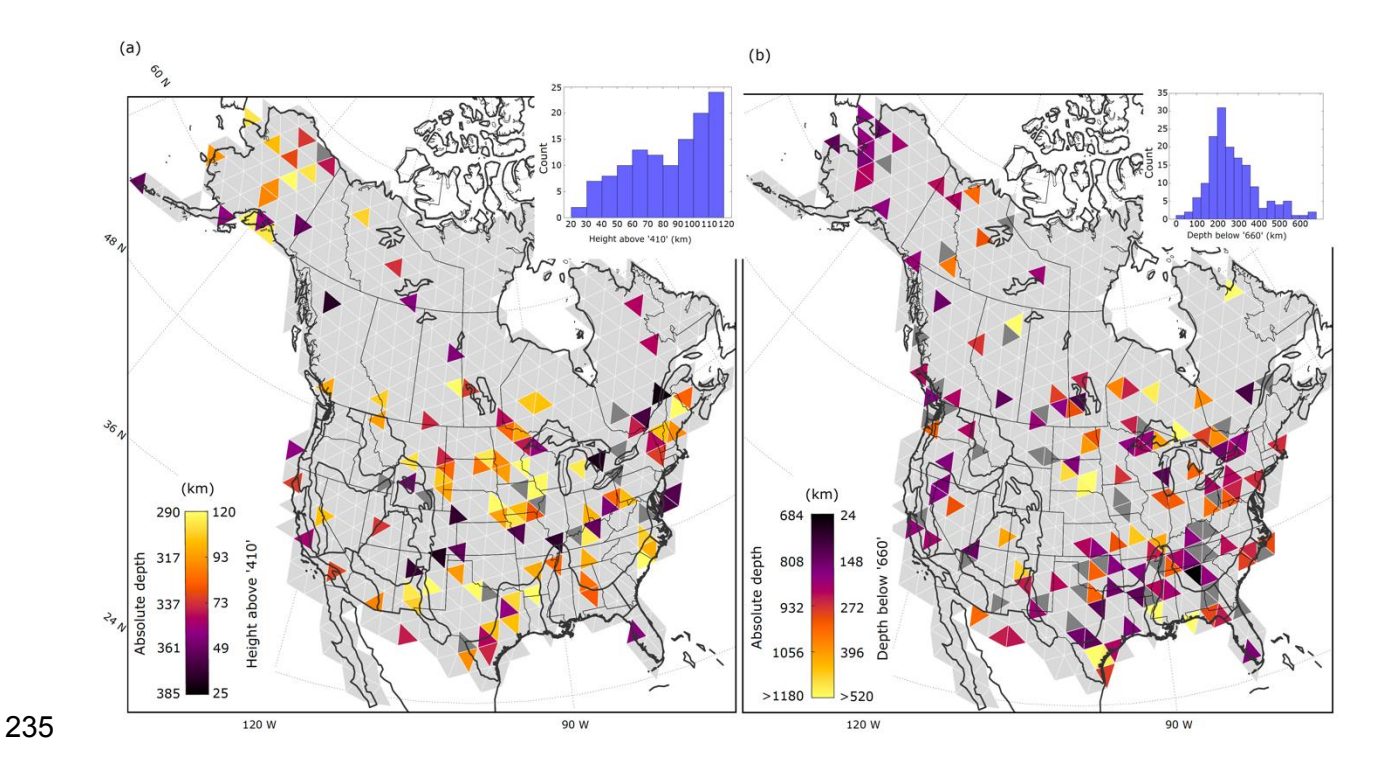


Figure 4. Mapping low-velocity discontinuities above and beneath the transition zone. (a, b) Depth maps of low-velocity discontinuities above the '410' and '660' discontinuities respectively. Insets display depth histograms for each discontinuity.

reflects half of regions with good data quality and coverage. Within this set, we found that majority of the detections are isolated to either the upper mantle or mid-mantle. For example, 91 out of 228 (~40%) of the cells record a detection exclusively above the MTZ and 101 out of 228 (~44%) solely below it. Only a small fraction of cells (8%) shows paired detection of discontinuities above and below the transition zone (blue triangles in Figure 5). The higher detection rate below the transition zone suggests that conditions are more favorable, in the mid-mantle beneath North America, for the formation of these features.

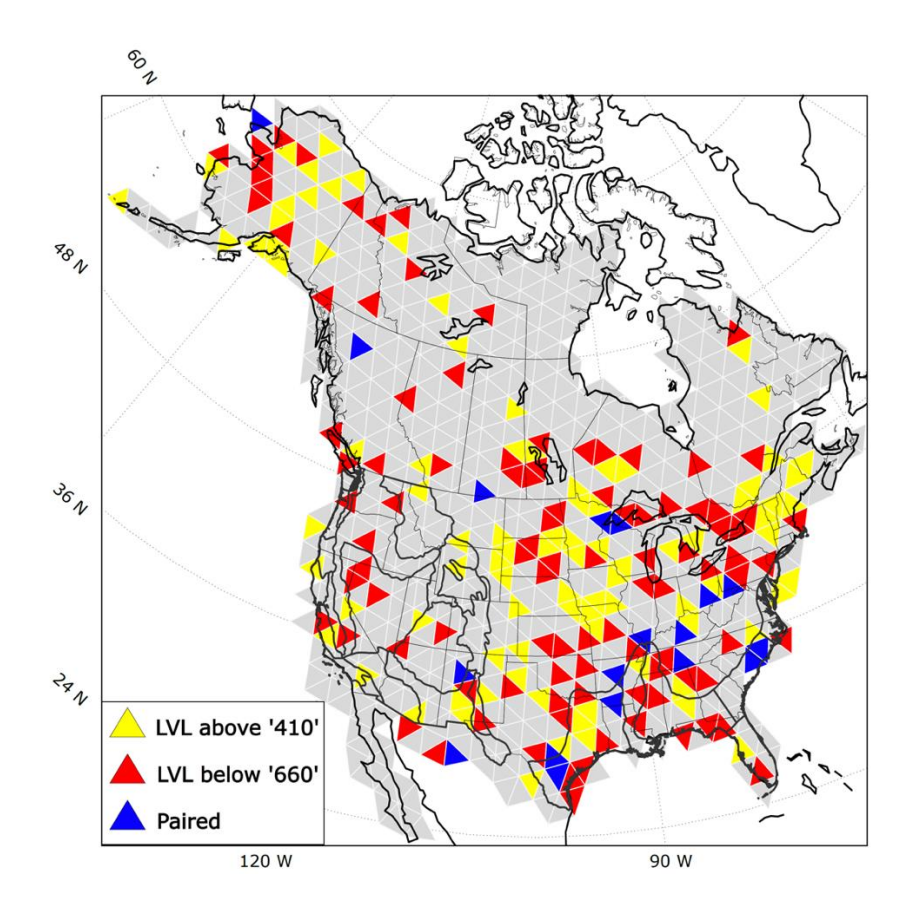


Figure 5. Spatial correlation of low-velocity discontinuities. The seemingly random distribution suggests no clear spatial correlation between upper mantle and mid-mantle LVDs across North America hinting at independent mechanisms governing their formation.

We summarize key findings on the spatial patterns of the discontinuity depth across a variety of different tectonic settings – from stable cratons in the continental interiors to areas with recent tectonic activity in Alaska and western US. Above the transition zone, the observed discontinuity depth varies from \sim 25–120 km (Figure 4a). A statistical analysis of this topography shows that the distribution is asymmetric, with a slight preference for depths between 317 km and 290 km (Figure 2b and inset of Figure 4a). A discontinuity located at \sim 290 km is more likely especially around the great plains in the US and in Alaska. Below the transition zone, distribution has a clear peak. This means that there is a higher probability of finding a mid-mantle discontinuity, \sim 225 km

O

below MTZ, at ~885 km. At a few stations, especially in the continental interiors of the US and Canada, the discontinuity is as deep as ~1,200 km. However, our data processing algorithm assesses the deepest LVD detections to have lower likelihood than most shallower detections. Taken together, we observe very little spatial correlation between the discontinuity topography above the transition zone relative to the bathymetry below it. This absence of a correlation suggests that the mechanisms responsible for generating these two discontinuities operate independent of each other.

4 Discussion

If our interpretations of CRISP-RF analyses in terms of low-velocity zones both above and below the mantle transition zone (MTZ) are correct, there are several implications for whole-earth geodynamics and geochemistry. Two leading hypotheses for large-scale mid-mantle processes are the basalt-enrichment hypothesis for incomplete mantle mixing (Frazer and Park, 2024; Tauzin et al., 2022; Yu et al., 2023), and the extension of the water-filter hypothesis (Bercovici and Karato, 2003) to a model for the long-term evolution of Earth's ocean mass with the MTZ as a reservoir of water (Karato et al., 2020). In the first hypothesis, subducted oceanic crust remains unmixed in Earth's mantle and likely forms local concentrations of eclogitic garnet- and iron-rich rock to generate 3-D seismic velocity variations in the mid mantle. In the second hypothesis, excess hydration of MTZ minerals wadsleyite and ringwoodite, both derived from upper-mantle olivine, leads to water release and partial melting whenever this material convects upward into the upper mantle or downward into the lower

mantle. In this scenario, water is released during the mineral phase changes and facilitates low-velocity zones from partial melting.

Evidence in favor of these two hypotheses initially took the form of global-average seismic models or regional seismic variations that are laterally broad. For example, (Anderson and Bass, 1986) invoked 1-D seismic models to argue for excess garnet in the mantle, relative to a pyrolite composition, and (Song et al., 2004) argued for an LVD above the 410-km discontinuity from perturbations to body-wave triplications where shear waves average properties along near-horizontal ray paths. However, with Ps receiver functions observed by dense arrays, (Liu et al., 2018, 2016) argued that LVDs of smaller lateral extent are induced by small-scale convective motions in areas of active subduction and lithospheric detachment, respectively, in NE Asia and the European Alps. Similarly, (Frazer and Park, 2021) found small LVDs about the MTZ linked to the upwelling Yellowstone hotspot system and the foundering Farallon slab. These studies anticipated the detection of isolated LVD patches that we describe across North America using CRISP-RF.

The small-scale features above and below the MTZ plotted in Figures 4 and 5 could reflect ongoing or fossil geodynamic processes in the middle mantle. If the seismic features identify patches of unmixed relict oceanic crust, the geodynamics are likely to be fossil, owing to the modest amount of active subduction within and at the margins of North America. Hedlin et al (1997) argued that PKP-precursor scattering was consistent with a mantle-wide distribution of weak (1%) wavespeed perturbations, with dominant scale length (8 km) comparable to the thickness of Earth's oceanic crust. The LVZ features that we detect could be local

Pg

amplifications of such wavespeed anomalies. Alternatively, if the seismic LVZ features identify regions where convecting MTZ rock has dehydrated, an ongoing process is theoretically possible, though we are unaware of other evidence that small-scale convection is pervasive across the 410-km and 660-km discontinuities in regions that lack active slabs and plumes. Patches of dehydration and partial melting, developed over the long history of plate tectonics on Earth could, however, persist in the mid-mantle as fossil anomalies. Karato et al (2020) argues that partial melts above the 410-km mineral phase changes would typically be denser than the residual solid, unless water content is high, and that partial melts below the 660-km would typically be lighter than the residual solid. Over long times, these melts should return to the mantle transition zone. The time scale for melt return is unknown, however, and will depend on the details of composition, relative buoyancy, and pore-space connectedness. It is possible that water is captured by high-pressure hydrous minerals in the upper and lower mantle that currently are not sampled at Earth's surface (Ishii et al., 2022; Ohtani, 2021; Tsuchiya and Thompson, 2022). By analogy with the elastic behavior of common hydrous minerals, these high-pressure hydrous phases could preserve a remnant seismic wavespeed anomaly, should be considered as explanations for localized persistent LVZ scatterers above and below the MTZ. Therefore, the widespread and disconnected regions of velocityinversion interfaces that we infer from CRISP-RF could be imagined as a volumetric landscape of past convective motions of hydrated MTZ rock into the hydrophobic upper and lower mantles.

Both above scenarios for 3-D mid-mantle heterogeneity may be active within Earth's interior and could combine to explain our observations. Does one process fit our observations better

304

305

306

307

308

309

310

311

312

313

314

315

316

317

318

319

320

321

322

323

324

than the other? Figure 2 argues for a near-continuous range of depths at which we detect these LVZ features, both above and below the MTZ. This behavior discourages an interpretation of these signals as a side-lobe of band passed seismic data (Frazer & Park, 2024) or as a static or steady-state phase change at a particular combination of temperature and pressure. It agrees, however, with the scenario where fluid-release-mediated partial melting is carried by convective motions away from the MTZ boundaries by varying distances. In this case the melt persists in the mid-mantle or solidifies into an assemblage of high-pressure hydrous minerals, and does not all return to the MTZ, at least not quickly. Based on equilibrium thermodynamics, small garnet-rich volumes of subducted oceanic crust should not have sharp preferences in depth, but the geodynamic modeling of (Yan et al., 2020) and (Yu et al., 2023) predict that garnet-rich heterogeneities should be relatively scarce between the 660-km discontinuity and 1000-km depth. We observe no such gap in the distribution of lower-mantle LVZ signals in our CRISP-RF results.

Our most powerful observation, however, may be the scarcity of locations in North America where we observe LVZ features both above and below the MTZ. When interpreted with binomial statistics over 228 independent detection locations beneath the densely instrumented regions, the probability that only 8% of these locations display paired LVZ detections is tiny (p<10-10). In most studies, one must allow for spatial correlation of detection locations, which can increase the probability substantially, but our CRISP-RF detections display minimal correlation both laterally and vertically.

Pg

A random distribution of eclogitic remnants within Earth's mantle has no obvious way to produce the observed scarcity of paired-LVZ detections that we observe. A scenario where hydrated MTZ material convects either upwards or downwards into a mineral phase-change that releases water seems more likely to display a local preference for seismic anomalies above or below the MTZ, but uncommonly both. In support of this scenario, we note that LVZ detections beneath the MTZ are frequent and more clustered in depth beneath Alaska and Western Canada than elsewhere in North America, consistent with recent downwelling associated the Pacific Northwest subduction zones. We conclude that our CRISP-RF results for North America are more consistent with seismic anomalies generated via the Karato et al (2020) scenario than the basalt-enrichment scenario of Tauzin et al (2022), with the proviso that water that escapes the MTZ may persist long-term in the lower and upper mantles within a few 100-km of the boundaries, and not readily return to the MTZ to maintain its hydration.

5 Conclusion

We present a comprehensive high-resolution mapping of North America's mid-mantle reflectivity using the CRISP-RF technique. We observe widespread low-velocity discontinuities above (~290 km to ~390 km depth) and below (~885 km, with some detections as deep as ~1,200 km) the mantle transition zone (MTZ) discontinuities. Only 8% of locations show paired LVD detections both above and below the MTZ, suggesting independent mechanisms for their formation. Our findings align more consistently with models of water transport and dehydration melting. This suggests that partial melting following mantle dehydration may persist long-term in the upper and mid-mantle within a few hundred kilometers of the transition zone discontinuities, or else forms high-pressure hydrous

minerals that maintain their seismic wavespeed anomalies. Our signal-processing approach opens new avenues for investigating mantle dynamics, the global water cycle, and the long-term evolution of the Earth's interior. In order to refine our understanding of mantle structure, future work should focus on extending high-resolution mapping globally.

6 Acknowledgements

This work was made possible with the support of the National Science Foundation under Grant 2339370. The authors acknowledge the use of the Bluehive Linux cluster at the University of Rochester's Center for Integrated Research Computing (CIRC). Seismic data are obtained from the Earth Scope Data Management Center. The authors acknowledge many helpful discussions with Vedran Lekic, Nicholas Schmerr, Baowei Liu, Sayan Swar, Ziqi Zhang and the anonymous reviewers.

379 References 380

- Anderson, D.L., Bass, J.D., 1986. Transition region of the Earth's upper mantle. Nature 320, 321–328. https://doi.org/10.1038/320321a0
- Ballmer, M.D., Schmerr, N.C., Nakagawa, T., Ritsema, J., 2015. Compositional mantle layering revealed by slab stagnation at~ 1000-km depth. Science advances.
- Bentham, H.L.M., Rost, S., 2014. Scattering beneath Western Pacific subduction zones: evidence for oceanic crust in the mid-mantle. Geophys. J. Int. 197, 1627–1641. https://doi.org/10.1093/gji/ggu043
- Bercovici, D., Karato, S.-I., 2003. Whole-mantle convection and the transition-zone water filter. Nature 425, 39–44. https://doi.org/10.1038/nature01918
- Boschi, L., Becker, T.W., 2011. Vertical coherence in mantle heterogeneity from global seismic data. Geophys. Res. Lett. 38. https://doi.org/10.1029/2011gl049281
- Carr, S.A.B., Olugboji, T., 2024. A taxonomy of upper-mantle stratification in the US. J. Geophys. Res. [Solid Earth] 129. https://doi.org/10.1029/2024jb028781
- Courtier, A.M., Revenaugh, J., 2008. Slabs and shear wave reflectors in the midmantle. J. Geophys. Res. 113. https://doi.org/10.1029/2007jb005261
- Deuss, A., Andrews, J., Day, E., 2013. Seismic observations of mantle discontinuities and their mineralogical and dynamical interpretation, in: Physics and Chemistry of the Deep Earth. John Wiley & Sons, Ltd, Chichester, UK, pp. 295–323. https://doi.org/10.1002/9781118529492.ch10
- Dziewonski, A.M., Anderson, D.L., 1981. Preliminary reference Earth model. Phys. Earth Planet. Inter. 25, 297–356. https://doi.org/10.1016/0031-9201(81)90046-7

- Fei, H., Ballmer, M.D., Faul, U., Walte, N., Cao, W., Katsura, T., 2023. Variation in bridgmanite grain size accounts for the mid-mantle viscosity jump. Nature 620, 794–799. https://doi.org/10.1038/s41586-023-06215-0
- Frazer, W.D., Park, J., 2024. No globally detectable seismic interfaces within Earth's mantle
 transition zone: Evidence for basalt enrichment. Earth Planet. Sci. Lett. 641, 118838.
 https://doi.org/10.1016/j.epsl.2024.118838
- Frazer, W.D., Park, J., 2021. Seismic evidence of mid-mantle water transport beneath the
 Yellowstone region. Geophys. Res. Lett. 48. https://doi.org/10.1029/2021gl095838
- Hedlin, M.A.H., Shearer, P.M., Earle, P.S., 1997. Seismic evidence for small-scale
 heterogeneity throughout the Earth's mantle. Nature 387, 145–150.
 https://doi.org/10.1038/387145a0
 - Helffrich, G., 2006. Extended-Time Multitaper Frequency Domain Cross-Correlation Receiver-Function Estimation. Bull. Seismol. Soc. Am. 96, 344–347. https://doi.org/10.1785/0120050098
- Helffrich, G.R., Wood, B.J., 2001. The Earth's mantle. Nature 412, 501–507.
 https://doi.org/10.1038/35087500
 - Hier-Majumder, S., Tauzin, B., 2017. Pervasive upper mantle melting beneath the western US. Earth Planet. Sci. Lett. 463, 25–35. https://doi.org/10.1016/j.epsl.2016.12.041
 - Ishii, T., Miyajima, N., Criniti, G., Hu, Q., Glazyrin, K., Katsura, T., 2022. High pressure-temperature phase relations of basaltic crust up to mid-mantle conditions. Earth Planet. Sci. Lett. 584, 117472. https://doi.org/10.1016/j.epsl.2022.117472
 - Jenkins, J., Deuss, A., Cottaar, S., 2017. Converted phases from sharp 1000 km depth midmantle heterogeneity beneath Western Europe. Earth Planet. Sci. Lett. 459, 196–207. https://doi.org/10.1016/j.epsl.2016.11.031
 - Kaneshima, S., 2023. Mid-mantle seismic scatterers beneath the Samoan hotspot. Phys. Earth Planet. Inter. 340, 107034. https://doi.org/10.1016/j.pepi.2023.107034
 - Kaneshima, S., 2019. Seismic scatterers in the lower mantle near subduction zones. Geophys. J. Int. https://doi.org/10.1093/gji/ggz241/29192106/ggz241
 - Kaneshima, S., 2018. Seismic scatterers in the mid-lower mantle beneath Tonga-Fiji. Phys. Earth Planet. Inter. 274, 1–13. https://doi.org/10.1016/j.pepi.2017.09.007
 - Kaneshima, S., 2016. Seismic scatterers in the mid-lower mantle. Phys. Earth Planet. Inter. 257, 105–114. https://doi.org/10.1016/j.pepi.2016.05.004
 - Karato, S.-I., Karki, B., Park, J., 2020. Deep mantle melting, global water circulation and its implications for the stability of the ocean mass. Progress in Earth and Planetary Science 7, 76. https://doi.org/10.1186/s40645-020-00379-3
- Kennett, B.L.N., Engdahl, E.R., Buland, R., 1995. Constraints on seismic velocities in the
 Earth from traveltimes. Geophys. J. Int. 122, 108–124.
 https://doi.org/10.1111/j.1365-246X.1995.tb03540.x
- Liu, Z., Park, J., Karato, S., 2016. Seismological detection of low-velocity anomalies
 surrounding the mantle transition zone in Japan subduction zone. Geophys. Res.
 Lett. 43, 2480–2487. https://doi.org/10.1002/2015gl067097
- Liu, Z., Park, J., Karato, S.-I., 2018. Seismic evidence for water transport out of the mantle
 transition zone beneath the European Alps. Earth Planet. Sci. Lett. 482, 93–104.
 https://doi.org/10.1016/j.epsl.2017.10.054

Pg

413

414

415

418

419

420

421

422

423

424

425

426

427

428

429

430

431

432

433

434

435

- Niu, F., 2014. Distinct compositional thin layers at mid-mantle depths beneath northeast China revealed by the USArray. Earth Planet. Sci. Lett. 402, 305–312. https://doi.org/10.1016/j.epsl.2013.02.015
- Niu, F., Kawakatsu, H., 1997. Depth variation of the mid-mantle seismic discontinuity.

 Geophys. Res. Lett. 24, 429–432. https://doi.org/10.1029/97gl00216
- Ohtani, E., 2021. Hydration and Dehydration in Earth's Interior. Annu. Rev. Earth Planet.
 Sci. 49, 253–278. https://doi.org/10.1146/annurev-earth-080320-062509
- Olugboji, T., Zhang, Z., Carr, S., Ekmekci, C., Cetin, M., 2023. On the detection of upper mantle discontinuities with radon-transformed receiver functions (CRISP-RF).

 Geophys. J. Int. 236, 748–763. https://doi.org/10.1093/gji/ggad447
- Park, J., Levin, V., 2016. Receiver Functions from Multiple-Taper Spectral Correlation:
 Statistics, Single-Station Migration, and Jackknife Uncertainty, Submitted to.
 Geophys. J. Int.
- 459 Park, J., Levin, V., 2000. Receiver Functions from Multiple-Taper Spectral Correlation
 460 Estimates. Bull. Seismol. Soc. Am. 90, 1507–1520.
 461 https://doi.org/10.1785/0119990122
- Revenaugh, J., Sipkin, S.A., 1994. Seismic evidence for silicate melt atop the 410-km mantle discontinuity. Nature 369, 474–476. https://doi.org/10.1038/369474a0
 - Rondenay, S., 2009. Upper Mantle Imaging with Array Recordings of Converted and Scattered Teleseismic Waves. Surv. Geophys. 30, 377–405. https://doi.org/10.1007/s10712-009-9071-5

464

465

466

467

468 469

470

471

- Rudolph, M.L., Lekić, V., Lithgow-Bertelloni, C., 2015. Viscosity jump in Earth's midmantle. Science 350, 1349–1352. https://doi.org/10.1126/science.aad1929
- Schmandt, B., Jacobsen, S.D., Becker, T.W., Liu, Z., Dueker, K.G., 2014. Dehydration melting at the top of the lower mantle. Science 344, 1265–1268. https://doi.org/10.1126/science.1253358
- Shen, Y., Wolfe, C.J., Solomon, S.C., 2003. Seismological evidence for a mid-mantle
 discontinuity beneath Hawaii and Iceland. Earth Planet. Sci. Lett. 214, 143–151.
 https://doi.org/10.1016/S0012-821X(03)00349-2
- Song, T.-R.A., Helmberger, D.V., Grand, S.P., 2004. Low-velocity zone atop the 410-km
 seismic discontinuity in the northwestern United States. Nature 427, 530–533.
 https://doi.org/10.1038/nature02231
- Stixrude, L., Lithgow-Bertelloni, C., 2012. Geophysics of Chemical Heterogeneity in the
 Mantle. Annual Review of Earth and.
 https://doi.org/10.1146/annurev.earth.36.031207.124244
- Tauzin, B., Debayle, E., Wittlinger, G., 2010. Seismic evidence for a global low-velocity layer
 within the Earth's upper mantle. Nat. Geosci. 3, 718–721.
 https://doi.org/10.1038/ngeo969
- Tauzin, B., van Der Hilst, R.D., 2013. Multiple transition zone seismic discontinuities and low velocity layers below western United States. Research: Solid Earth.
- Tauzin, B., Waszek, L., Ballmer, M.D., Afonso, J.C., Bodin, T., 2022. Basaltic reservoirs in the Earth's mantle transition zone. Proceedings of the National Academy of Sciences 119, e2209399119. https://doi.org/10.1073/pnas.2209399119

- Tian, D., Lv, M., Wei, S.S., Dorfman, S.M., Shearer, P.M., 2020. Global variations of Earth's
 520- and 560-km discontinuities. Earth Planet. Sci. Lett. 552, 116600.
 https://doi.org/10.1016/j.epsl.2020.116600
- Tsuchiya, J., Thompson, E.C., 2022. The role of hydrogen bonds in hydrous minerals stable at lower mantle pressure conditions. Progress in Earth and Planetary Science 9, 63. https://doi.org/10.1186/s40645-022-00521-3

495 496

497

498

499

500

501

502

503

504

505

506

507

508

509

513

- Waszek, L., Schmerr, N.C., Ballmer, M.D., 2018. Global observations of reflectors in the mid-mantle with implications for mantle structure and dynamics. Nat. Commun. 9, 385. https://doi.org/10.1038/s41467-017-02709-4
- Yan, J., Ballmer, M.D., Tackley, P.J., 2020. The evolution and distribution of recycled oceanic crust in the Earth's mantle: Insight from geodynamic models. Earth Planet. Sci. Lett. 537, 116171. https://doi.org/10.1016/j.epsl.2020.116171
- Yang, Z., He, X., 2015. Oceanic crust in the mid-mantle beneath west-central Pacific subduction zones: evidence from S to P converted waveforms. Geophys. J. Int. 203, 541–547. https://doi.org/10.1093/gii/ggv314
- Yu, C., Goes, S., Day, E.A., van der Hilst, R.D., 2023. Seismic evidence for global basalt accumulation in the mantle transition zone. Sci Adv 9, eadg0095. https://doi.org/10.1126/sciadv.adg0095
 - Zhang, Z., Irving, J.C.E., Simons, F.J., Alkhalifah, T., 2023. Seismic evidence for a 1000 km mantle discontinuity under the Pacific. Nat. Commun. 14, 1714. https://doi.org/10.1038/s41467-023-37067-x
- Zhang, Z., Olugboji, T., 2024. Crustal Imaging with Noisy Teleseismic Receiver Functions
 Using Sparse Radon Transforms. Bull. Seismol. Soc. Am.
 https://doi.org/10.1785/0120230254